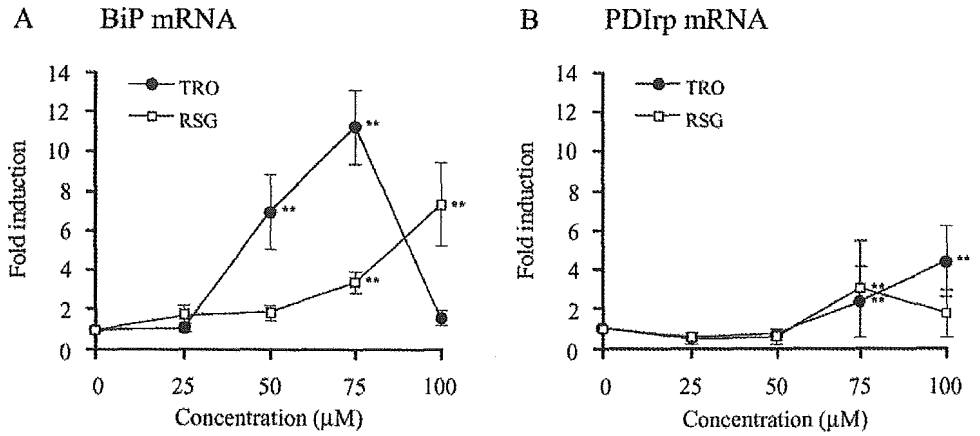

FIG. 5. Changes of BiP and PDIrp mRNA expression by TZDs in HepG2 cells. HepG2 cells were incubated with 0.1% DMSO (control) or the indicated concentrations of TRO or RSG for 48 h. The cDNA were prepared for real-time PCR. Sense and antisense primers of BiP (5′-TGCTTGATGTATGTCCCCTTA-3′ and 5′-CCTTGTCTTCAGCTGTCACT-3′) and PDIrp (5′-AATACCAGGATGCCGCTAAC-3′ and 5′-GCAAAGGTGTACTCAGGGAA-3′) were used. The relative BiP and PDIrp expression values were normalized with the GAPDH values of the same samples. The data represent the mean ± SD of three independent experiments. $^{**}p < 0.01$ compared with the control.

effects, an RNA interference technique was carried out for knockdown BiP expression. Because of the difficulty in transfecting siRNA into HepG2 cells, human hepatoma HLE cells were used instead. In our previous report, TRO possessed toxic effects on HLE cells as well as HepG2 cells, but with somewhat higher sensitivity (Yamamoto *et al.*, 2001). The BiP mRNA expression in HLE cells treated with TRO and RSG showed a similar pattern to that in HepG2 cells (data not shown). Compared to mock-transfected cells, BiP expression with DMSO treatment (control) was diminished by 50 and 100 nM of siRNA by about 30 and 17%, respectively. Furthermore, when additionally treated with 75 μM of TRO, the BiP mRNA was dramatically suppressed from 16-fold to 1.7- and 1.6-fold, respectively (Fig. 6A). Similarly, in siRNA-transfected cells treated with 100 μM of RSG, the BiP mRNA was suppressed from 2.5-fold to 0.6- and 1.0-fold, respectively (Fig. 6A). The BiP protein expression was also investigated in HLE cells after transfection with 50 nM BiP siRNA and subsequent treatment with TRO and RSG at concentrations of 75 and 100 μM, respectively. Figure 6B shows the inhibition of BiP protein production compared to the mock-transfected control under both control (DMSO) and treatment conditions assessed by Western blot analyses.

Cell Viability Changes by Troglitazone Treatment in BiP-Suppressed Cells

BiP inhibition by siRNA was clearly demonstrated, especially in the presence of TRO and RSG, to be superior to that of the mock-transfected control. Accordingly, HLE cells were then investigated in terms of the phenotypic changes. The ATP-based luminescent assay was used to measure the cell viability. In the DMSO-treated control there was a dose-dependent decrease in cell viability by BiP siRNA transfection (Fig. 7A), whereas there were no significant changes by lamin A siRNA, a negative control of siRNA transfection (Fig. 7B). Interestingly, 50 μM TRO treatments caused a significant decrease in cell viability with 10 nM of BiP siRNA ($p < 0.05$) and a marked decreased ($p < 0.01$) at the high concentration of 25 to 100 nM of BiP siRNA compared to the DMSO-treated control (Fig.7A). The 75 μM TRO treatment demonstrated significant toxic effects ($p < 0.01$) in all BiP siRNA-transfected concentrations including the mock-transfected cells (transfected control). RSG at the concentration of 75 and 100 μM showed comparable results with the DMSO with both BiP siRNA and lamin A siRNA transfection (Figs. 7A and 7B).

DISCUSSION

The toxicological potential of TRO compared to that of another TZD agent, RSG, was investigated in a human hepatoma cell line, HepG2. In this study, TRO treatment showed concentration-dependent cytotoxicity with an approximate IC_{50} of 40 μM, whereas only a slight decrease in cell viability was found with RSG treatment (Fig. 1A). These results were consistent with the previous reports, which additionally revealed that the lethal effects are exemplified by apoptosis (Bae *et al.*, 2003; Bae and Song, 2003; Yamamoto *et al.*, 2001). In our findings, the toxic effects of TRO in HepG2 cells were also exhibited in a time-dependent manner (Fig. 1B) and were significantly observed from 24 h of exposure. Although RSG showed a significant decrease in cell viability from 48 h to 60 h ($p < 0.05$), cell viabilities were more than 80% of the control

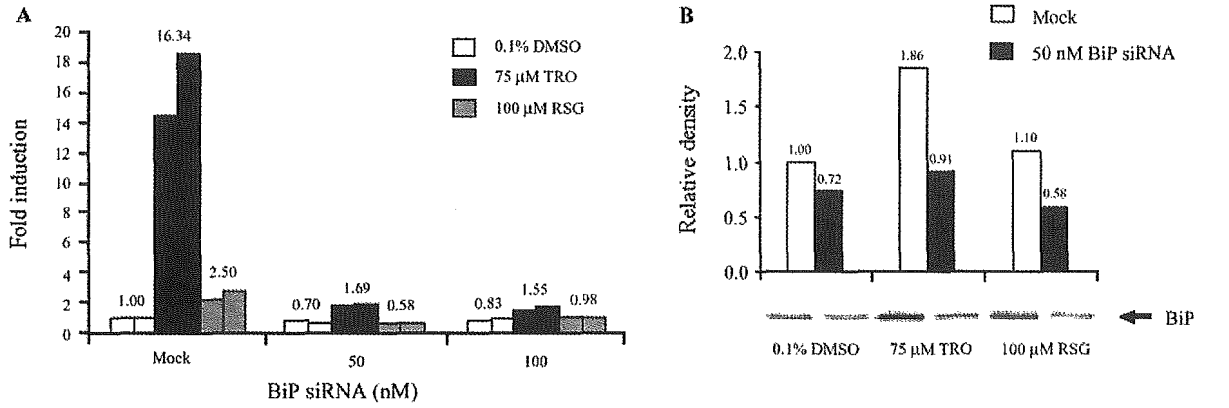

FIG. 6. Inhibitory effects of BiP siRNA on the BiP mRNA and protein expression. (A) HLE cells were transfected with 50 or 100 nM of BiP siRNA for 24 h. TRO or RSG was added to the transfection medium to make a final concentration of 75 μM or 100 μM, respectively. DMSO (0.1%) treatment was used as a control. The cells were further incubated for 24 h. The cDNA was prepared for real-time PCR. Sense and antisense primers of BiP (5′-TGCT-TGATGTATGTCCCCTTA-3′ and 5′-CCTTGTCTTCAGCTGTCACT-3′) were used. The relative BiP expression values were normalized with the GAPDH values of the same samples. (B) HLE cells were transfected with 50 nM of BiP siRNA for 24 h. TRO or RSG was added to the transfection medium to make a final concentration of 75 μM or 100 μM, respectively. DMSO (0.1%) treatment was used as a control. The cells were further incubated for 24 h. The cell lysates were prepared and subjected to Western blot analysis with mouse anti-KDEL antibody for detecting BiP protein. The expression of BiP protein was measured using a densitometer. The data represent the average value of duplicate determinations.

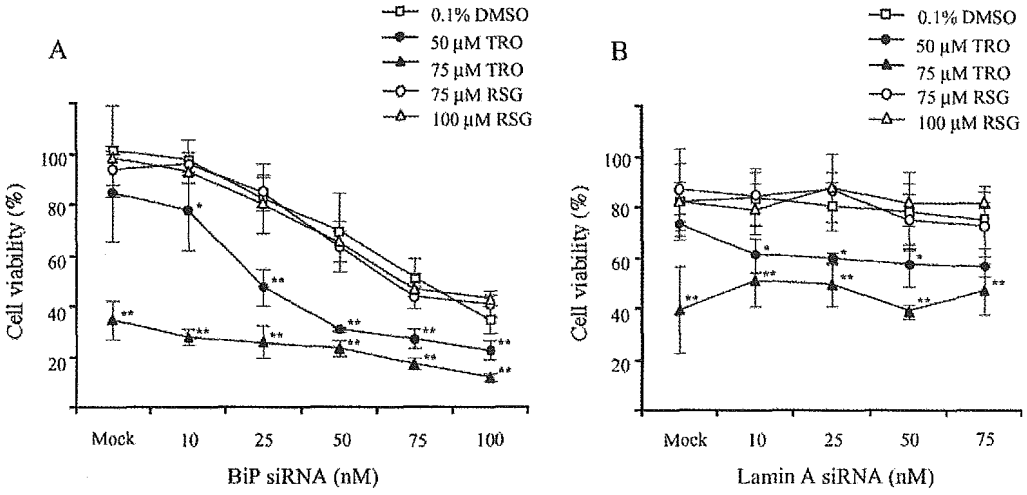

FIG. 7. Effects of BiP inhibition on cell viability. HLE cells were transfected with various concentrations of BiP siRNA (A) or lamin A siRNA as the negative control (B) for 24 h. TRO or RSG was added to the transfection medium to make a final concentration as indicated. DMSO (0.1%) treatment was used as a control. The cells were further incubated for 24 h. Cell viabilities were determined by ATP-based luminescent assay as described in Materials and Methods. The cell viability values were calculated with cell viability of the non-treated cells as 100% (neither transfection reagent nor TZDs). The data represent the mean ± SD of at least three independent experiments. $*p < 0.05$, $**p < 0.01$ compared with the control.

(Fig. 1B). The crystal violet assay in our protocol could not detect the time-dependent cytotoxicity, because the cells were not adherent before 24 h after seeding. We also confirmed with the trypan blue exclusion assay in a time-course experiment from 4 to 60 h. The percent cell viabilities were comparable to those detected with crystal violet, and significant lethal effects were observed from 12 to 60 h by 50 μM TRO exposure (data not shown). TRO has been reported to be metabolized to three main metabolites: sulfate-conjugated, glucuronide-conjugated, and quinone-type (TRO quinone) metabolites (Izumi *et al.*, 1997a,b; Kawai *et al.*, 1998). TRO, but not RSG, contains a 6-hydroxy-5,7,8-trimethylchromane moiety, which undergoes metabolic activation by hepatic cytochrome P450 enzymes, CYP2C8 and CYP 3A4, to generate TRO quinone (Tettey *et al.*, 2001; Yamazaki *et al.*, 1999). Based on the general involvement of quinones in cytotoxicity, TRO quinone has been reported to have a possible association with TRO-induced hepatotoxicity (Neuschwander-Tetri *et al.*, 1998). Previously, we

found a major epoxide of the quinone metabolite of TRO in HepG2 cells (Yamamoto *et al.*, 2002). However, the toxicity possessed by either TRO quinone or the epoxide of TRO quinone is relatively lower than that of the parent compound (Tettey *et al.*, 2001; Yamamoto *et al.*, 2001, 2002). Thus, the hepatotoxic effects were more likely due to TRO or other unknown metabolites.

Since the remarkable cytotoxicity of TRO has been established, we used 2-DE to investigate the protein expression profiles of HepG2 cells treated with various concentrations of TRO or RSG. On 2-D gels, more than ten different spots according to the treatments were revealed (small part shown in Fig. 2). We focused on a spot of interest at an approximate MW of 75 kDa and isoelectric point of 5, which showed distinct dose-dependency and TRO-specific changes with the greatest expression. The protein spot was highly matched with BiP and also, to a lesser extent, PDIrp (Fig. 3). These proteins are recognized as chaperone proteins that reside in the ER (Gething and Sambrook, 1992).

BiP, known as a 78 kDa glucose-regulated protein (Grp78), is related to the highly conserved 70 kDa heat shock protein (hsp70) family (Munro and Pelham, 1986). Apart from its response to heat, BiP is also the best-characterized chaperone and is abundantly and constitutively expressed in the ER of all eukaryotic cells (Gething and Sambrook, 1992; Haas, 1994). This protein is responsible for normal cellular functions such as assisting protein folding, assembly, and disassembly for maintenance, as well as the degradation of untenable proteins. BiP production can be induced by various perturbations of ER functions such as the expression of mutant proteins or protein subunits, reductive stress, ER Ca^{2+} depletion, and the inhibition of asparagine (N)-linked glycosylation (Gething and Sambrook, 1992; Haas, 1994; Kaufman, 1999, Lee, 2001). In our study, TRO treatment elicited a dose-dependent overexpression of BiP protein, as confirmed by Western blot analyses (Fig. 4A). BiP mRNA was also induced by treatment with 50 and 75 μM of TRO (Fig. 5A). At 100 μM TRO treatment, which resulted in about 15% cell viability, the highest induction of BiP protein was observed, but not the mRNA. Gülow *et al.* (2002) reported that under ER stress conditions, BiP expression is tightly controlled post-transcriptionally, allowing the cells to produce more proteins which are independent from the transcription level. As shown in Figure 6B, we confirmed that, with the inhibition of BiP mRNA expression before TRO or RSG treatment, the induction of BiP protein could not be achieved. Thus, the effects of 100 μM TRO treatment could be in part explained by the high translation efficiency of BiP protein in HepG2 cells. In our observation, RSG treated-HepG2 cells also induced BiP expression but at a low level, which would account for its lower toxicity compared to TRO.

Protein disulfide isomerase-related protein (herein referred to as PDIrp), or 72 kDa endoplasmic reticulum protein (ERp72), is also a resident chaperone in the ER which shares amino acid sequences with ERp59 (PDI) and holds three copies of the thioredoxin active unit as well as PDI activity *in vitro* (Gething and Sambrook, 1992; Mazzarella *et al.*, 1990). In normal cells, PDIrp is expressed constitutively at low levels and is induced by the same treatments that affect BiP expression (Huang *et al.*, 1989). We found PDIrp close to the BiP spot. However, unlike BiP, PDIrp protein was expressed equally in all treatments (Fig. 4B). Given the similar characteristics between PDIrp and PDI (Mazzarella *et al.*, 1990), we also investigated the PDI protein level in the same set of treated samples using its specific antibody. Indeed, the PDI protein expression showed comparable results (Fig. 4C) to PDIrp. Although a small induction of PDIrp mRNA was observed at the high doses of 75 and 100 μM, neither treatment lead to the overproduction of the protein. These present data suggest that the damage caused by TRO treatment was unlikely related to the increased PDI proficiency.

In order to confirm the prominent regulation of BiP by TRO-induced cytotoxicity, the RNA interference method was applied to HLE, another human hepatoma cell line. In the condition of siRNA transfection with TRO treatment, BiP expression was suppressed by about 90% compared to the corresponding mock-transfected cells (Fig.6A). This finding was reflected by the phenotypic change in cell viability. TRO caused changes in the permeability and structure of mitochondria as well as a depletion of ATP, which were correlated with the decrease of cell viability (Tirmenstein *et al.*, 2002). With a small amount of cells, the luminescent assay was considered to be sufficiently sensitive to detect the relative ATP (Fig. 1C) and showed parallel results with the cell viability in Figure 1A. Thus, to observe the phenotypic changes caused by the TRO-induced suppression of BiP, ATP produced by metabolically active cells was used as a biomarker in this study. Comparing the results in Figures 7A and 7B, we found that the inhibition of BiP appeared to promote cell death even in the absence of TRO. This supports the crucial function of BiP in normal cellular processes (Gething and Sambrook, 1992; Haas, 1994; Kaufman, 1999). Doses of 50 and 75 μM TRO as well as 75 and 100 μM RSG, which caused the high levels of BiP mRNA expression, were used. Interestingly, in the presence of 50 μM TRO, the inhibition of BiP expression rendered cells more susceptible to the lethality, as demonstrated by a gradual increase in significant cell toxicity along with the increase in the concentration of BiP siRNA (Fig. 7A). Supporting this finding, a related study reported that inhibition of BiP synthesis sensitizes cells to oxidative stress (Liu *et al.*, 1998). These phenotypic changes in cell viability suggested the crucial role of BiP overexpression in the effects of TRO exposure.

It is well known that ER is a major cellular storage site of Ca^{2+} in the cell, and ER chaperones also play important roles in Ca^{2+} accumulation and release. Both BiP and PDIrp are Ca^{2+}-binding proteins (Lee, 2001). Any disturbance in the ER homeostasis causes a release of Ca^{2+}, which in turn blocks ER protein processing, resulting in the accumulation of incompletely folded proteins, and activates the transcription of ER chaperone genes including *BiP* (Liu *et al.*, 1998; Lodish and Kong, 1990).

In previous reports, TRO but not RSG exhibited antiproliferative effects on cultured cells via a depletion of Ca^{2+} from the storage site that results in the inhibition of translation initiation (Fan *et al.*, 2004; Palakurthi *et al.*, 2001). Together with our results, it might be postulated that TRO acts as a chemical signal that causes the release of Ca^{2+} from the ER, and that BiP expression is one of the cellular responses induced by TRO toxicity. In addition, the effects of TRO on the activation of JNK pathway (Bae and Song, 2003), disturbance of mitochondria function, and depletion of ATP (Tirmenstein *et al.*, 2002) may also converge in the ER stress response (Breckenridge *et al.*, 2003).

In conclusion, the possibility was raised in the present study that the ER is one of the targets involved in TRO hepatotoxicity. TRO may serve as a stress signal to the ER, which in turn causes the overproduction of BiP in response to cytotoxicity. Supporting this view, the inhibition of BiP at the post-transcriptional level sensitized the cells to lethality.

ACKNOWLEDGMENTS

This work was supported in part by a grant from the Ministry of Education, Science, Sports, and Culture of Japan, and by Research on Advanced Medical Technology and Welfare of Japan. We thank Mr. Brent Bell for reading the manuscript.

REFERENCES

Bae, M. A., Rhee, H., and Song, B. J. (2003). Troglitazone but not rosiglitazone induces G1 cell cycle arrest and apoptosis in human and rat hepatoma cell lines. *Toxicol. Lett.* **139,** 67–75.

Bae, M. A., and Song, B. J. (2003). Critical role of c-Jun N-terminal protein kinase activation in troglitazone-induced apoptosis of human HepG2 hepatoma cells. *Mol. Pharmacol.* **63,** 401–408.

Breckenridge, D. G., Germain, M., Mathai, J. P., Nguyen, M., and Shore, G. C. (2003). Regulation of apoptosis by endoplasmic reticulum pathways. *Oncogene* **22,** 8608–8618.

Fan, Y. H., Chen, H., Natarajan, A., Guo, Y., Harbinski, F., Iyasere, J., Christ, W., Aktas, H., and Halperin, J. A. (2004). Structure-activity requirements for the antiproliferative effect of troglitazone derivatives mediated by depletion of intracellular calcium. *Bio. Med. Chem. Lett.* **14,** 2547–2550.

Freid, J., Everitt, D., and Boscia, J. (2000). Rosiglitazone and hepatic failure. *Ann. Intern. Med.* **132,** 164.

Fujiwara, T., Yoshioka, S., Yoshioka, T., Ushiyama, I., and Horikoshi, H. (1988). Characterization of new oral antidiabetic agent CS-045, Studies in *KK* and *ob/ob* mice and Zucker fatty rats. *Diabetes* **37,** 1549–1558.

Gething, M. J., and Sambrook, J. (1992). Protein folding in the cell. *Nature* **355,** 33–45.

Gitlin, N., Julie, N. L., Spurr, C. L., Lim, K. N., and Juarbe, H. M. (1998). Two cases of severe clinical and histologic hepatotoxicity associated with troglitazone. *Ann. Intern. Med.* **129,** 36–38.

Gülow, K., Bienert, D., and Haas, I. G. (2002). BiP is feed-back regulated by control of protein translation efficiency. *J. Cell Sci.* **115,** 2443–2452.

Haas, I. G. (1994). BiP (GRP78), an essential hsp70 resident protein in the endoplasmic reticulum. *Experientia* **50,** 1012–1020.

Huang, S. H., Tomich, J. M., Wu, H., Jong, A., and Holcenberg, J. (1989). Human deoxycystidine kinase, sequence of cDNA clones and analysis of expression in cell lines with and without enzyme activity. *J. Biol. Chem.* **264,** 14762–14768. Erratum in: *J. Biol. Chem.* **266,** 5353.

Isley, W. L., and Oki, J. C. (2000). Rosiglitazone and liver failure. *Ann. Intern. Med.* **133,** 393.

Izumi, T., Enomoto, S., Hoshiyama, K., Sasahara, K., and Sugiyama, Y. (1997a). Pharmacokinetic stereoselectivity of troglitazone, an antidiabetic agent, in the KK mouse. *Biopharm. Drug Dispos.* **18,** 305–324.

Izumi, T., Hoshiyama, K., Enomoto, S., Sasahara, K., and Sugiyama, Y. (1997b). Pharmacokinetics of troglitazone, an antidiabetic agent: Prediction of *in vivo* stereoselective sulfation and glucuronidation from *in vitro* data. *J. Pharmacol. Exp. Ther.* **280,** 1392–1400.

Kaufman, R. J. (1999). Stress signaling from the lumen of the endoplasmic reticulum: Coordination of gene transcriptional and translational control. *Genes Dev.* **13,** 1211–1233.

Kawai, K., Odaka, T., Tsurata, F., Tokui, T., Ikeda, T., and Nakamura, K. (1998). Stereoselective metabolism of new oral anti-diabetic agent troglitazon estereoisomers in liver. *Xenobio. Metab. Dispos.* **13,** 362–368.

Lebovitz, H. E., Kreider, M., and Freed, M. I. (2002). Evaluation of liver function in type 2 diabetic patients during clinical trials. *Diabetes Care* **25,** 815–821.

Lee, A. S. (2001). The glucose-regulated proteins: Stress induction and clinical applications. *Trends Biochem. Sci.* **26,** 504–510.

Lehmann, J. M., Moore, L. B., Smith-Oliver, T. A., Wilkison, W. O., Willson, T. M., and Kliewer, S. A. (1995). An antidiabetic thiazolidinedione is a high affinity ligand for peroxisome-activated receptor γ (PPARγ). *J. Biol. Chem.* **270,** 12953–12956.

Liu, H., Miller, E., van de Water, B., and Stevens, J. L. (1998). Endoplasmic reticulum stress proteins block oxidant-induced Ca^{2+} increases and cell death. *J. Biol. Chem.* **273,** 12858–12862.

Lodish, H. F., and Kong, N. (1990). Perturbation of cellular calcium blocks exit of secretory proteins from the rough endoplamic reticulum. *J. Biol. Chem.* **265,** 10893–10899.

Mazzarella, R. A., Srinivasan, M., Haugejorden, S. M., and Green, M. (1990). ERp72, an abundant luminal endoplasmic reticulum protein, contains three copies of the active site sequences of protein disulfide isomerase. *J. Biol. Chem.* **265,** 1094–1101.

Munro, S., and Pelham, H. R. B. (1986). An Hsp70-like protein in the ER: Identity with the 78 kD glucose-regulated protein and immunoglobulin heavy chain binding protein. *Cell* **46,** 291–300.

Nakagawa, T., Sawada, M., Gonzalez, F. J., Yokoi, T., and Kamataki, T. (1996). Stable expression of human CYP2E1 in Chinese hamster cells: High sensitivity to *N,N*-dimethylnitrosamine in cytotoxicity testing. *Mutat. Res.* **360,** 181–186.

Neuschwander-Tetri, B. A., Isley, W. L., Oki, J. C., Ramrakhiani, S., Quiason, S. G., Phillips, N. J., and Brunt, E. M. (1998). Troglitazone-induced hepatic failure leading to liver transplantation. *Ann. Intern. Med.* **129,** 38–41.

Nolan, J. J., Ludvik, B., Beerdsen, P., Joyce, M., and Olefsky, J. (1994). Improvement in glucose tolerance and insulin resistance in obese subjects treated with troglitazone. *N. Engl. J. Med.* **331,** 1188–1193.

Palakurthi, S. S., Aktas, H., Grubissich, L. M., Mortensen, R. M., and Halperin, J. A. (2001). Anticancer effects of thaiazolidinediones are independent of peroxisome proliferators-activated receptor γ and mediated by inhibition of translation initiation. *Cancer Res.* **61,** 6213–6218.

Rothwell, C., McGuire, E. J., Altrogge, D. M., Masuda, H., and de la Iglesia, F. A. (2002). Chronic toxicity in monkeys with the thiazolidinedione antidiabetic agent troglitazone. *J. Toxicol. Sci.* **27,** 35–47.

Shibuya, A., Watanabe, M., Fujita, Y., Saigenji, K., Kuwao, S., Takahashi, H., and Takeuchi, H. (1998). An autopsy case of troglitazone-induced fulminant hepatitis. *Diabetes Care* **21,** 2140–2143.

Tettey, J. N., Maggs, J. L., Rapeport, W. G., Pirmohamed, M., and Park, B. K. (2001). Enzyme induction dependent bioactivation of troglitazone and troglitazone quinone *in vivo*. *Chem. Res. Toxicol.* **14,** 965–974.

Tirmenstein, M. A., Hu, C. X., Gales, T. L., Maleeff, B. E., Narayanan, P. K., Kurali, E., Hart, T. K., Thomas, H. C., and Schwartz, L. W. (2002). Effects of troglitazone on HepG2 viability and mitochondrial function. *Toxicol. Sci.* **69,** 131–138.

Watanabe, T., Ohashi, Y., Yasuda, M., Takaoka, M., Furukawa, T., Yamoto, T., Sanbuissho, A., and Manabe, S. (1999). Was it possible to predict liver dysfunction caused by troglitazone during the nonclinical safety studies? *Iyakuhin Kenkyu* **30,** 537–546.

Watkins, P. B., and Whitcomb, R. W. (1998). Hepatic dysfunction associated with troglitazone. *N. Engl. J. Med.* **338,** 916–917.

Yamamoto, Y., Nakajima, M., Yamazaki, H., and Yokoi, T. (2001). Cytotoxicity and apoptosis produced by troglitazone in human hepatoma cells. *Life Sci.* **70,** 471–482.

Yamamoto, Y., Yamazaki, H., Ikeda, T., Watanabe, T., Iwabuchi, H., Nakajima, M., and Yokoi, T. (2002). Formation of a quinone epoxide metabolite of troglitazone with cytotoxic to HepG2 cells. *Drug Metab. Dispos.* **30,** 155–160.

Yamazaki, H., Shibata, A., Suzuki, M., Nakajima, M., Shimada N., Guengerich, F. P., and Yokoi, T. (1999). Oxidation of troglitazone to a quinone-type metabolite catalyzed by cytochrome P-450 2C8 and P-450 3A4 in human liver microsomes. *Drug Metab. Dispos.* **27,** 1260–1266.

Xenobiotica, June 2005; 35(6): 549–560

Taylor & Francis
Taylor & Francis Group

Inhibitory effects of psychotropic drugs on mexiletine metabolism in human liver microsomes: Prediction of *in vivo* drug interactions

Y. HARA[1,2], M. NAKAJIMA[1], K.-I. MIYAMOTO[2], & T. YOKOI[1]

[1]*Drug Metabolism and Toxicology, Division of Pharmaceutical Sciences, Graduate School of Medical Science, Kanazawa University, Kanazawa, Japan, and*
[2]*Kanazawa University Hospital, Kanazawa, Japan*

(Received 17 February 2005)

Abstract

Mexiletine, an anti-arrhythmic agent, is used for the control of ventricular arrhythmias and for neuropathic pain from cancer or diabetes mellitus. It is sometimes used together with psychotropic drugs in patients with depression, schizophrenia or sleep disorder. It is metabolized mainly by cytochrome P450 (CYP) 2D6 and, to a minor extent, by CYP1A2. To predict possible drug interactions between mexiletine and psychotropic drugs, the inhibitory effects of 14 psychotropic drugs (phenytoin, carbamazepine, fluvoxamine, paroxetine, fluoxetine, citalopram, sertraline, imipramine, desipramine, haloperidol, thioridazine, olanzapine, etizolam, and quazepam) on mexiletine metabolism in human liver microsomes were determined. Fluoxetine ($K_i = 0.6 \pm 0.1\,\mu M$), sertraline ($K_i = 7.6 \pm 0.8\,\mu M$) and desipramine ($K_i = 3.2 \pm 0.5\,\mu M$) competitively inhibited the mexiletine *p*-hydroxylation in human liver microsomes. Thioridazine ($K_{is} = 0.5 \pm 0.2\,\mu M$; $K_{ii} = 3.6 \pm 1.6\,\mu M$) and paroxetine ($K_{is} = 1.7 \pm 0.7\,\mu M$; $K_{ii} = 3.6 \pm 0.9\,\mu M$) exhibited a mixed-type inhibition (competitive and non-competitive) toward mexiletine *p*-hydroxylation in human liver microsomes. The changes of the *in vivo* clearance of mexiletine by the psychotropic drugs were predicted by $1 + (I/K_i)$ using the *in vitro* K_i and unbound inhibitor concentrations in liver. The values were calculated as 2.4 for paroxetine, 5.5 for fluoxetine, 1.1 for sertraline, 2.8 for desipramine and 2.2 for thioridazine. In addition, paroxetine exhibited a mechanism-based inactivation with $K_i = 0.7\,\mu M$ and $K_{inact} = 0.15\,min^{-1}$. The present study predicted the possibility of drug interactions between mexiletine and paroxetine, fluoxetine, desipramine, and thioridazine in clinical use.

Keywords: *Mexiletine, cytochrome P450, psychotropic drug, inhibition, inactivation*

Correspondence: T. Yokoi, Drug Metabolism and Toxicology, Division of Pharmaceutical Sciences, Graduate School of Medical Science, Kanazawa University, Kakuma-machi, Kanazawa 920-1192, Japan. Tel/Fax: 81-76-234-4407. E-mail: TYOKOI@kenroku.kanazawa-u.ac.jp

ISSN 0049-8254 print/ISSN 1366-5928 online © 2005 Taylor & Francis
DOI: 10.1080/00498250500158134

Introduction

Mexiletine is a class 1B anti-arrhythmic agent used for the control of ventricular arrhythmias and its anti-arrhythmic activity and toxicity are highly correlated with the plasma concentration of mexiletine and its therapeutic index is narrow (Campbell et al. 1978). Mexiletine is also used for the treatment of neuropathic pain from cancer and diabetes mellitus. In addition, 10–30% of cancer patients have psychological distress (Kugaya et al. 2000; Okamura et al. 2000; Akechi et al. 2001; Uchitomi et al. 2003). In the diabetic population, 24% of patients have depression (Goldney et al. 2004). Thus, mexiletine is sometimes used together with psychotropic drugs in patients with schizophrenia, depression and sleep disorders. There is abundant literature on the pharmacokinetic interactions between psychotropic drugs (Gram et al. 1974; Cooper et al. 1979; Lane 1996; Kurtz et al. 1997; Preskorn 1998). Almost all of those are due to the inhibition of cytochrome P450 (CYP) 2D6, which is a major metabolic enzyme for such psychotropic drugs. Mexiletine is metabolized to pharmacologically inactive *p*-hydroxymexiletine and 2-hydroxymexiletine mainly by CYP2D6 and, to a minor extent, by CYP1A2 (Nakajima et al. 1998). Therefore, the possibility of an interaction between mexiletine and psychotropic drugs should be considered. To predict the *in vivo* drug interactions, the present study investigated the inhibitory effects of psychotropic drugs on mexiletine metabolism in human liver microsomes. We selected 14 psychotropic drugs (phenytoin, carbamazepine, fluvoxamine, paroxetine, fluoxetine, citalopram, sertraline, imipramine, desipramine, haloperidol, thioridazine, olanzapine, quazepam and etizolam) (Figure 1) that may possibly be co-administered with mexiletine.

Materials and methods

Chemicals and reagents

Mexiletine [1-(2,6-dimethylphenoxy)-2-aminopropane] hydrochloride and *p*-hydroxymexiletine [1-(2,6-dimethyl-4-hydroxyphenoxy)-2-aminopropane] hydrochloride were kindly provided by Nippon Boehringer Ingelheim (Hyogo, Japan). Phenytoin, carbamazepine, imipramine hydrochloride, desipramine hydrochloride and haloperidol were purchased from Wako Chemicals (Tokyo, Japan). 5-Methoxyindol 3-acetic acid and fluoxetine were purchased from Sigma-Aldrich (St Louis, MO, USA). Fluvoxamine maleate was from Tocris Cookson (Ballwin, MO, USA). Paroxetine hydrochloride, citalopram, sertraline and olanzapine were purchased from Toronto Research Chemicals (Toronto, Canada). Thioridazine hydrochloride was kindly provided by Novartis Pharma AG (Basel, Switzerland). Quazepam and etizolam were kindly supplied by Mitsubishi Pharma (Osaka, Japan). $NADP^+$, glucose 6-phosphate, and glucose 6-phosphate dehydrogenase were from Oriental Yeast (Tokyo, Japan). Pooled human liver microsomes were obtained from BD Gentest (Woburn, MA, USA). All other chemicals were of the highest grade commercially available.

Mexiletine hydroxylase activity

Mexiletine hydroxylase activity in human liver microsomes was determined as reported (Nakajima et al. 1998). A typical incubation mixture (0.2 ml total volume) contained 100 mM potassium phosphate buffer (pH 7.4), an NADPH-generating system (0.5 mM $NADP^+$, 5 mM glucose 6-phosphate, 5 mM $MgCl_2$, 1 U ml^{-1} glucose 6-phosphate dehydrogenase), 0.5 mg ml^{-1} microsomal protein and mexiletine as a substrate. Each psychotropic drug, which was dissolved in methanol, was added as an inhibitor so that the

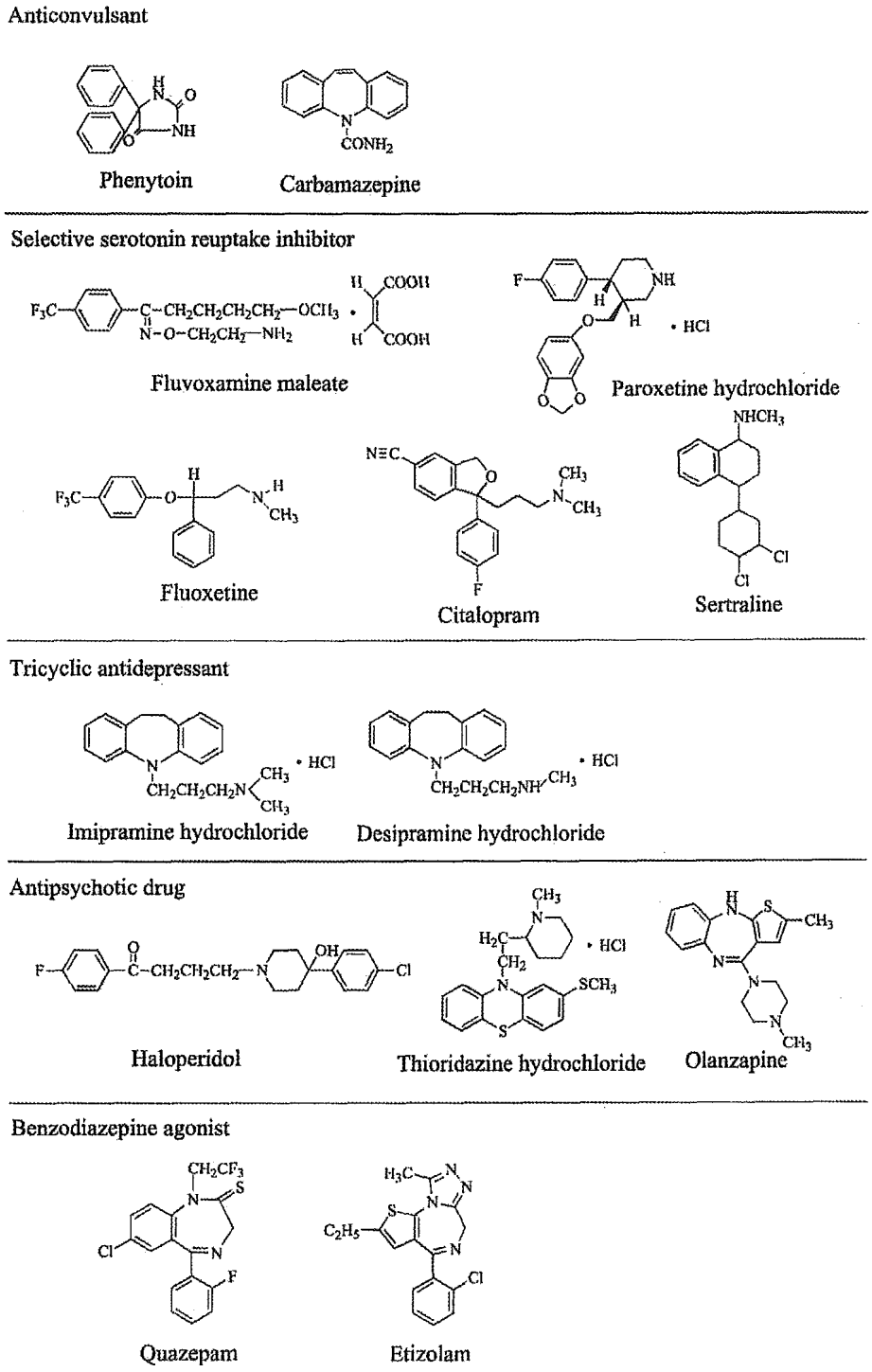

Figure 1. Structures of the psychotropic drugs used.

final concentration of solvent in the incubation mixture was <1%. The reaction was initiated by the addition of the NADPH-generating system following a 2-min pre-incubation at 37°C. The reaction was terminated by the addition of 0.1 ml ice-cold methanol, and 5-methoxyindole 3-acetic acid (10 ng) was added as an internal standard. After the removal

of protein by centrifugation at 10 000*g* for 5 min, a 100-μl portion of the supernatant was subjected to HPLC. Chromatography was performed using an L-2130 pump, an L-2480 FL detector, an L-2200 autosampler, a D-2500 integrator and an L-2300 column oven (Hitachi, Tokyo, Japan). The flow rate was 1.0 ml min^{-1} and the column temperature was 35°C. The hydroxylated metabolites were detected fluorometrically (excitation 270 nm, emission 312 nm) with a noise-base clean Uni-3 (Union, Gunma, Japan). The analytical column was a Capcell Pak C_{18} UG120 (4.6 × 250 mm; 5 μm) column (Shiseido, Tokyo, Japan) and the mobile phase was 10% acetonitrile containing 10 mM potassium dihydrogen phosphate (pH 4.5). The retention times of *p*-hydroxymexiletine, 2-hydroxymexiletine, 5-methoxyindole 3-acetic acid and mexiletine were 8.5, 11.0, 31.0 and 50.0 min, respectively. The quantification of the metabolite was performed by comparing the HPLC peak heights with that of authentic standard with reference to the internal standard.

Mechanism-based inactivation of human CYPs by paroxetine

Human liver microsomes were pre-incubated at 37°C for 10, 20 and 30 min with various concentrations of paroxetine (0.13, 0.25 and 0.50 μM final concentrations) in the presence of an NADPH-generating system. After pre-incubation, the mexiletine hydroxylase activities at a 20 μM substrate concentration were measured according to the method described above. Kinetic parameters of the inactivation process, k_{inact} and K_i, were calculated as described (Nakajima et al. 1999).

Data analyses

Lineweaver–Burk plots were used for the determination of the type of inhibition (Segel 1993), and Dixon plots were used as a secondary method. Kinetic parameters were determined by non-linear regression analysis using a computer program (K-cat, BioMetallics, Princeton, NJ, USA). All data were analysed using the average of duplicate determinations.

Prediction of interaction at clinical doses from in vitro *data*

If an enzyme reaction is inhibited competitively by other drugs, the velocity (V) is expressed as follows:

$$V = V_{max}\frac{S}{\{K_m(1+[I/K_i])+S\}}$$

where I and S are the concentration of the inhibitor and substrate, respectively. When the substrate concentration is much lower than K_m ($K_m \gg S$), the change in the intrinsic clearance (CL_{int}) is expressed as follows:

$$\frac{CL_{int}(+\text{inhibitor})}{CL_{int}(-\text{inhibitor})} = \frac{1}{(1+[I_u/K_i])}$$

where I_u is the unbound concentration of the inhibitor and K_i is the inhibition constant. When we discuss drug–drug interactions via inhibition of CYP, it is important that the concentration of the inhibitor refers to the concentration of the drug at CYP. It is difficult to know the actual concentrations of drugs at the active site of CYP. In the present study, the changes of CL_{int} caused by psychotropic drugs were predicted using the maximum

unbound concentrations in the liver estimated by the plasma concentration and protein binding. Since the protein binding of each psychotropic drug in tissues has not been reported, we assumed that these are the same as the protein binding in plasma.

Results

Inhibition of mexiletine p-*hydroxylase activity in human liver microsomes by psychotropic drugs*

The major metabolic pathways of mexiletine in humans are aromatic hydroxylation, forming *p*-hydroxymexiletine and aliphatic hydroxylation, forming 2-hydroxymexiletine. We previously reported that the kinetics and the contribution ratio of CYP2D6/CYP1A2 for *p*-hydroxylation and 2-hydroxylation are almost the same (Nakajima et al. 1998), i.e. the K_m values for mexiletine *p*-hydroxylation in recombinant CYP2D6 and CYP1A2 were 22.6 and 13.9 μM, respectively; the V_{max} values for mexiletine *p*-hydroxylation in CYP2D6 and CYP1A2 were 2249 and 4.7 fmol min^{-1} $pmol^{-1}$ CYP, respectively; the K_m values for mexiletine 2-hydroxylation in recombinant CYP2D6 and CYP1A2 were 22.1 and 15.2 μM, respectively; the V_{max} values for mexiletine 2-hydroxylation in CYP2D6 and CYP1A2 were 2492 and 6.1 fmol min^{-1} $pmol^{-1}$ CYP, respectively. Since *p*-hydroxymexiletine is more easily detected than 2-hydroxymexiletine with HPLC because of the higher absorbance coefficient, mexiletine *p*-hydroxylation in human liver microsomes was monitored in the present study.

The psychotropic drugs (100 μM) were screened for the inhibitory effects on mexiletine *p*-hydroxylase activity at a 10 μM mexiletine concentration (lower than K_m). As shown in Figure 2, mexiletine *p*-hydroxylase activity was completely abolished by paroxetine and thioridazine. In addition, 100 μM fluoxetine (17% of control), sertraline (12%) and desipramine (16%) extensively inhibited mexiletine *p*-hydroxylase activity. The IC_{50} values were 0.5 μM for paroxetine, 0.6 μM for thioridazine, 1.0 μM for fluoxetine, 11.0 μM for sertraline and 5.4 μM for desipramine (data not shown).

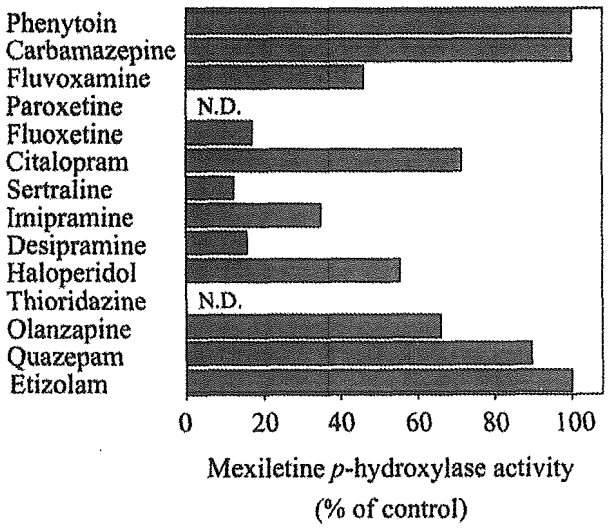

Figure 2. Inhibitory effects of psychotropic drugs on mexiletine *p*-hydroxylase activity in human liver microsomes. The concentrations of mexiletine and each psychotropic drug were 10 and 100 μM, respectively. Each column is the average of duplicate determinations. The control activity in the pooled human liver microsomes was 2.6 pmol min^{-1} mg^{-1} protein. N.D., not detected.

Inhibition constant and inhibition pattern

We determined the inhibition constants (K_i) for the compounds that exhibited extensive inhibition (Figure 3). The K_{is} and K_{ii} values are inhibition constants on the slope (competitive) and on the intercept (non-competitive), respectively. Paroxetine exhibited

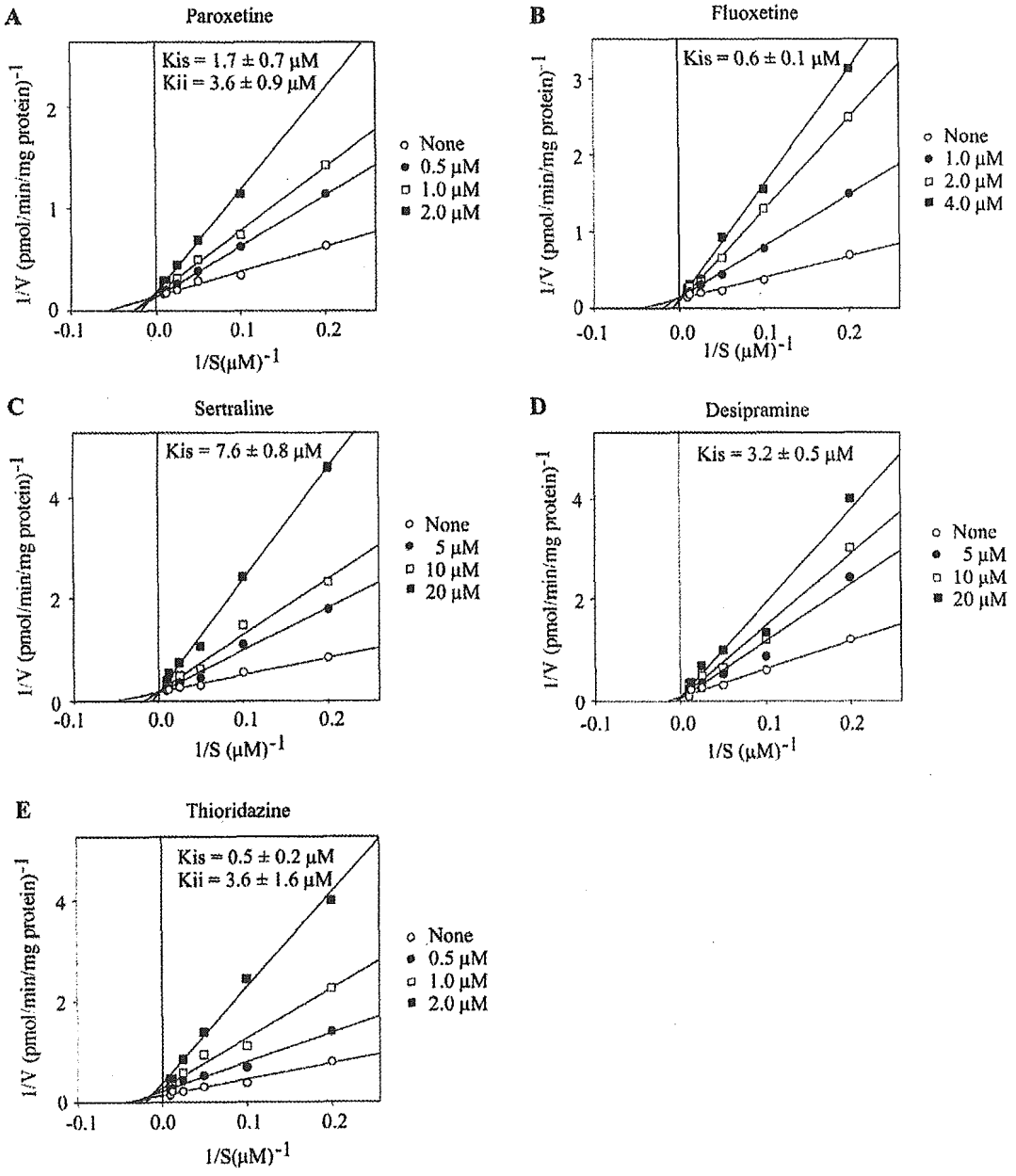

Figure 3. Lineweaver–Burk plots of mexiletine *p*-hydroxylase activity in human liver microsomes. Effects of (A) paroxetine, (B) fluoxetine, (C) sertraline, (D) desipramine and (E) thioridazine on mexiletine *p*-hydroxylase activity in human liver microsomes are shown. Each datum point is the average of duplicate determinations. Lines were drawn by linear regression analysis. Paroxetine and thioridazine showed mixed-type (competitive and non-competitive) inhibition and the others showed competitive inhibition. K_{is} is the inhibition constant on the slope (competitive); K_{ii} is the inhibition constant on the intercept (non-competitive).

Table I. Predicted change of *in vivo* clearance of mexiletine by psychotropic drugs.

Psychotropic drugs	I_{max} (μM)	Protein binding (%)	I_u (nM)	$I_{u,liver}$ (μM)	K_i (μM)	$1+I_{u,liver}/K_i$
Paroxetine	1.5	95	75	2.3	1.7[a]	2.4
Fluoxetine	1.5	94	90	2.7	0.6	5.5
Sertraline	0.6	98	12	0.4	7.6	1.1
Desipramine	1.1	83	187	5.6	3.2	2.8
Thioridazine	1.6	98	32	0.6	0.5[a]	2.2

[a]In the case of mixed-type inhibition, the lower K_m was used in the calculation.

mixed-type inhibition with $K_{is} = 1.7 \pm 0.7$ μM and $K_{ii} = 3.6 \pm 0.9$ μM. Fluoxetine, sertraline and desipramine exhibited competitive inhibition with $K_{is} = 0.6 \pm 0.1$, 7.6 ± 0.8 and 3.2 ± 0.5 μM, respectively. Thioridazine also exhibited mixed-type inhibition with $K_{is} = 0.5 \pm 0.2$ μM and $K_{ii} = 3.6 \pm 1.6$ μM.

Predicted change of clearance of mexiletine by psychotropic drugs from in vitro *data*

To predict the possibility of drug interaction via a metabolic process between mexiletine and the psychotropic drugs, $1 + (I/K_i)$ values were calculated (Table I). The maximum plasma concentrations of paroxetine (Kaye et al. 1989), fluoxetine (Altamura et al. 1994), sertraline (DeVane et al. 2002), desipramine (Sallee and Pollock 1990) and thioridazine (Vanderheeren and Muusze 1977; Chakraborty et al. 1989) have been reported to be 1.5, 1.5, 0.6, 1.1 and 1.6 μM, respectively. The protein binding of each psychotropic drug in plasma has been reported to be 95% for paroxetine (Kaye et al. 1989), 94% for fluoxetine (Altamura et al. 1994), 98% for sertraline (DeVane et al. 2002), 83% for desipramine (Sallee and Pollock 1990) and 98% for thioridazine (Nyberg et al. 1978). In the liver, the concentrations of paroxetine, fluoxetine (Vermeulen 1998), desipramine (Apple and Bandt 1988) and sertraline (Levine et al. 1994) have been reported to be 30-fold higher that those in plasma. Thioridazine accumulation in the liver is 20-fold higher than the plasma concentration (Dinovo et al. 1978). Accordingly, the maximum unbound liver concentrations were estimated to be 2.3 μM for paroxetine, 2.7 μM for fluoxetine, 0.4 μM for sertraline, 5.6 μM for desipramine and 0.6 μM for thioridazine. Finally, the $1 + (I/K_i)$ values calculated for paroxetine, fluoxetine, sertraline, desipramine and thioridazine were 2.4, 5.5, 1.1, 2.8 and 2.2, respectively.

Mechanism-based inactivation of human CYP enzymes

Since paroxetine has a methylenedioxy moiety in the structure, we investigated the possibility that it functions as a mechanism-based inactivator. As shown in Figure 4, paroxetine inhibited mexiletine *p*-hydroxylase activities in human liver microsomes with the NADPH-generating system in a time- and concentration-dependent manner. $K_{inact} = 0.15\ min^{-1}$ and $K_i = 0.72$ μM (Figure 4). Thioridazine did not exhibit mechanism-based inactivation (data not shown). Fluoxetine, desipramine and sertraline were not investigated since these compounds have no structure that would suggest mechanism-based inactivation.

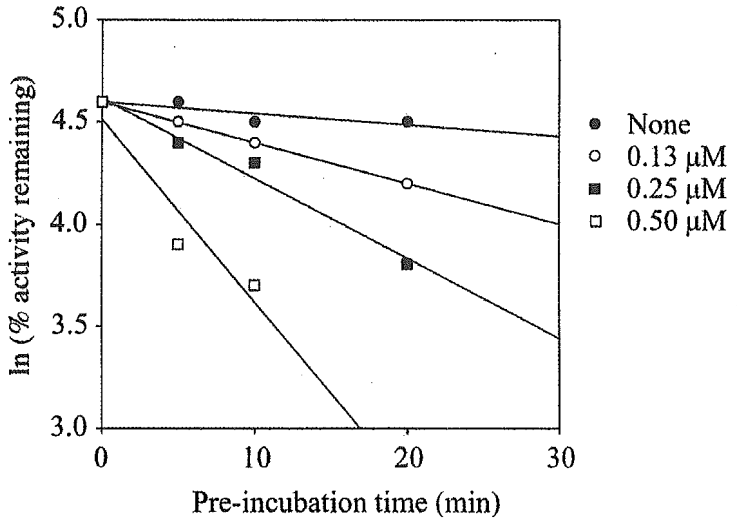

Figure 4. Mechanism-based inactivation of mexiletine *p*-hydroxylase activity in human liver microsomes by paroxetine. Pooled human liver microsomes were pre-incubated with various concentrations of paroxetine for 5, 10 and 20 min at 37°C in the presence of an NADPH-generating system. After pre-incubation, mexiletine was added to the reaction mixture and the *p*-hydroxymexiletine formed was determined. Lines were determined by linear regression of time versus the logarithm of the reaction velocity ratio. The concentration of mexiletine was 20 μM and the control activity was 3.4 pmol min^{-1} mg^{-1} protein. Data points represent the average of duplicate determinations.

Discussion

Mexiletine, an anti-arrhythmic drug, is sometimes used with psychotropic drugs in clinical practice. It has been reported that approximately 5% of the absorbed dose is excreted unchanged in human urine (Labbé and Turgeon 1999). Mexiletine is extensively metabolized, with metabolic ratios calculated as AUC of metabolite/AUC of mexiletine for *p*-hydroxymexiletine and 2-hydroxymexiletine ranging from 0.2 to 0.5 in humans (Paczkowski et al. 1990; Otani et al. 2003). It is well known that inhibition of drug metabolism of certain drugs by co-administered drugs might cause adverse reactions (Guengerich 1997; Lin and Lu 1998). Since the kinetics and the enzymes responsible for *p*-hydroxylation and 2-hydroxylation of mexiletine are almost the same (Nakajima et al. 1998), potent inhibition of mexiletine *p*-hydroxylation would imply substantial changes of *in vivo* mexiletine pharmacokinetics. In the present study, to predict the *in vivo* drug interactions between mexiletine and psychotropic drugs, the inhibitory effects of psychotropic drugs on mexiletine metabolism in human liver microsomes were investigated.

Phenytoin (metabolized mainly by CYP2C9 and to a minor extent by CYP2C19) (Bajpai et al. 1996) and carbamazepine (metabolized by CYP3A4) (Kerr et al. 1994) are anticonvulsant drugs. They are used as palliatives for lancinating pain such as trigeminal neuralgia and intractable neuropathic pain, and are sometimes used together with mexiletine. Selective serotonin re-uptake inhibitors such as fluvoxamine (metabolized by CYP2D6 and an inhibitor of CYP1A2 and CYP2C19) (Brosen et al. 1993; Harten 1995), paroxetine (metabolized by CYP2D6) (Bloomer et al. 1992), fluoxetine (metabolized mainly by CYP2D6 and to a minor extent by CYP2C9 and CYP3A4) (Fjordside et al. 1999; Margolis et al. 2000), citalopram (metabolized mainly by CYP3A4 and to a minor extent by CYP2C19)

(Kobayashi et al. 1997) and sertraline (metabolized by multiple isoforms of CYP2D6, CYP2C9, CYP2B6, CYP2C19 and CYP3A4) (Kobayashi et al. 1999; DeVane et al. 2002) are the most often prescribed antidepressants in many countries. Imipramine (metabolized by CYP2D6) (Skjelbo and Brosen 1992) and desipramine (metabolized by CYP2D6) (Von Moltke et al. 1995) are tricyclic antidepressants. Haloperidol (metabolized by CYP3A4) (Fang et al. 1997; Pan et al. 1997), a dopamine D2 receptor antagonist, is prescribed worldwide as a high-potency antipsychotic drug for the treatment of acute and chronic schizophrenia and other psychiatric disorders. Thioridazine (metabolized mainly by CYP2D6 and to minor extent by CYP2C19 and CYP1A2) (Vanderheeren and Muusze 1977; Eap et al. 1996; Carrillo et al. 1999) is piperidene-type phenothiazine that is widely used for the treatment of acute schizophrenia and related disorders. Olanzapine (metabolized mainly by UDP-glucuronosyltransferase and CYP1A2, and to a minor extent by CYP2D6) (Ring et al. 1996; Callaghan et al. 1999) is a new antipsychotic drug with a thiobenzodiazepinyl structure that is effective in the treatment of both positive and negative symptoms of schizophrenia. Quazepam and etizolam are benzodiazepine agonists that are frequently prescribed as anxiolytic and hypnoticum drugs. It has been reported that the plasma concentrations of these drugs are increased with co-administration of itraconazole, a potent CYP3A4 inhibitor (Kato et al. 2003; Araki et al. 2004).

In the present study, it was found that paroxetine ($K_i = 1.7\,\mu M$), fluoxetine ($0.6\,\mu M$), sertraline ($7.6\,\mu M$), desipramine ($3.2\,\mu M$) and thioridazine ($0.5\,\mu M$) extensively inhibited mexiletine metabolism in human liver microsomes. Mexiletine is mainly metabolized by CYP2D6 in human liver microsomes (Nakajima et al. 1998). Thus, it is reasonable to propose that psychotropic drugs that have the potential to inhibit CYP2D6 would affect mexiletine metabolism. According to the prediction of the change in the clearance of mexiletine *in vivo* from the *in vitro* data using the equation $1 + (I/K_i)$, it was found that the inhibitory effects of sertraline on mexiletine metabolism would be clinically insignificant. In contrast, it appeared that fluoxetine, desipramine, paroxetine and thioridazine could significantly inhibit mexiletine metabolism, possibly causing adverse effects such as tremors, diplopia, nausea and vomiting. In particular, the pharmacokinetic drug interaction between fluoxetine and mexiletine could result in severe adverse reactions. In the present study, bindings of the psychotropic drugs in the microsomal incubation were not considered when the K_i values were calculated. Therefore, in the case that the binding in the microsomal incubation is high, one should mind a possibility of underestimating the drug interactions.

On the other hand, psychotropic drugs may cause serious cardiovascular adverse effects such as prolonged QT interval. The risk of such adverse effects is high in individuals with a history of arrhythmias and may be potentiated by pharmacokinetic interactions with co-administered drugs (Brown et al. 2004). Mexiletine may cause ventricular tachycardia as an adverse reaction. Thus, drug interactions between mexiletine and psychotropic drugs such as paroxetine, fluoxetine, desipramine and thioridazine might be more complicated.

The mechanism-based inactivation of CYP in which a metabolite covalently binds to the enzyme to form a complex leads to irreversible inhibition (Silverman 1998). Compounds containing a methylenedioxy moiety, tertiary amine, furan ring or acetylene possibly become mechanism-based inactivators of CYP. Paroxetine has a methylenedioxy moiety in its structure. The methylenedioxy group results in the generation of carbene intermediates, which form a strong covalent complex with the iron centre of haem in CYP (Ortiz de Montellano and Correia 1995). In the present study, paroxetine inactivated the mexiletine *p*-hydroxylase activity in human liver microsomes with a $K_i = 0.72\,\mu M$ and

$k_{inact} = 0.15\,min^{-1}$. The inactivation potency was stronger than its effects on dextromethorphan demethylase in human liver microsomes ($K_i = 4.85\,\mu M$, $k_{inact} = 0.17\,min^{-1}$) that have been reported by Bertelsen et al. (2003). Once an enzyme is inactivated by a mechanism-based inactivator, the recovery of the metabolic activity depends on the synthesis of the enzyme. Thus, the turnover rate of the enzyme is one of the most important parameters in the prediction of interactions involving mechanism-based inactivation. There have been a few reports on successful predictions of *in vivo* interaction based on mechanism-based inactivation from *in vitro* data (Kanamitsu et al. 2000; Mayhew et al. 2000; Ito et al. 2003). Unfortunately, since the information on the turnover rate of most human enzymes is limited, the prediction of *in vivo* interaction by mechanism-based inactivation is difficult. Nevertheless, our data suggested that paroxetine could exhibit extensive inhibition of mexiletine metabolism as both a competitive inhibitor and mechanism-based inactivator, leading to prolonged and severe adverse effects.

In conclusion, among the 14 psychotropic drugs examined, paroxetine, fluoxetine, desipramine and thioridazine were predicted to cause drug interactions with mexiletine, which may result in adverse effects in clinical practice for patients taking mexiletine. It is important to select psychotropic drugs carefully to avoid possible drug interactions.

Acknowledgement

The authors acknowledge Mr Brent Bell for reviewing the manuscript.

References

Akechi T, Okamura H, Nishiwaki Y, Uchitomi Y. 2001. Psychiatric disorders and associated and predictive factors in patients with unresectable non small cell lung carcinoma: A longitudinal study. Cancer 92:2609–2622.

Altamura AC, Moro AR, Percudani M. 1994. Clinical pharmacokinetics of fluoxetine. Clinical Pharmacokinetics 26:201–214.

Apple FS, Bandt CM. 1988. Liver and blood postmortem tricyclic antidepressant concentrations. American Journal of Clinical Pathology 89:794–796.

Araki K, Yasui N, Fukasawa T, Aoshima T, Suzuki A, Inoue Y, Tateishi T, Otani K. 2004. Inhibition of the metabolism of etizolam by itraconazole in humans: Evidence for the involvement of CYP3A4 in etizolam metabolism. European Journal of Clinical Pharmacology 60:427–430.

Bajpai M, Roskos LK, Shen DD, Levy RH. 1996. Roles of cytochrome P4502C9 and cytochrome P4502C19 in the stereoselective metabolism of phenytoin to its major metabolite. Drug Metabolism and Disposition 24:1401–1403.

Bertelsen KM, Venkatakrishnan K, Von Moltke LL, Obach RS, Greenblatt DJ. 2003. Apparent mechanism-based inhibition of human CYP2D6 in vitro by paroxetine: Comparison with fluoxetine and quinidine. Drug Metabolism and Disposition 31:289–293.

Bloomer JC, Woods FR, Haddock RE, Lennard MS, Tucker GT. 1992. The role of cytochrome P4502D6 in the metabolism of paroxetine by human liver microsomes. British Journal of Clinical Pharmacology 33:521–523.

Brosen K, Hansen JG, Nielsen KK, Sindrup SH, Gram LF. 1993. Inhibition by paroxetine of desipramine metabolism in extensive but not in poor metabolizers of sparteine. European Journal of Clinical Pharmacology 44:349–355.

Brown CS, Farmer RG, Soberman JE, Eichner SF. 2004. Pharmacokinetic factors in the adverse cardiovascular effects of antipsychotic drugs. Clinical Pharmacokinetics 43:33–56.

Callaghan JT, Bergstrom RF, Ptak LR, Beasley CM. 1999. Olanzapine. Pharmacokinetic and pharmacodynamic profile. Clinical Pharmacokinetics 37:177–193.

Campbell NP, Kelly JG, Adgey AA, Shanks RG. 1978. The clinical pharmacology of mexiletine. British Journal of Clinical Pharmacology 6:103–108.

Carrillo JA, Ramos SI, Herraiz AG, Llerena A, Agundez JA, Berecz R, Duran M, Benitez J. 1999. Pharmacokinetic interaction of fluvoxamine and thioridazine in schizophrenic patients. Journal of Clinical Psychopharmacology 19:494–499.

Chakraborty BS, Midha KK, McKay G, Hawes EM, Hubbard JW, Korchinski ED, Choc MG, Robinson WT. 1989. Single dose kinetics of thioridazine and its two psychoactive metabolites in healthy humans: A dose proportionality study. Journal of Pharmaceutical Sciences 78:796–801.

Cooper SF, Dugal R, Elie R, Albert JM. 1979. Metabolic interaction between amitriptyline and perphenazine in psychiatric patients. Progress in Neuropsychopharmacology 3:369–376.

DeVane CL, Liston HL, Markowitz JS. 2002. Clinical pharmacokinetics of sertraline. Clinical Pharmacokinetics 41:1247–1266.

Dinovo EC, Bost RO, Sunshine I, Gottschalk LA. 1978. Distribution of thioridazine and its metabolites in human tissues and fluids obtained postmortem. Clinical Chemistry 24:1828–1830.

Eap CB, Guentert TW, Schaublin-Loidl M, Stabl M, Koeb L, Powell K, Baumann P. 1996. Plasma levels of the enantiomers of thioridazine, thioridazine 2-sulfoxide, thioridazine 2-sulfone, and thioridazine 5-sulfoxide in poor and extensive metabolizers of dextromethorphan and mephenytoin. Clinical Pharmacology and Therapeutics 59:322–331.

Fang J, Baker GB, Silverstone PH, Coutts RT. 1997. Involvement of CYP3A4 and CYP2D6 in the metabolism of haloperidol. Cellular and Molecular Neurobiology 17:227–233.

Fjordside L, Jeppesen U, Eap CB, Powell K, Baumann P, Brosen K. 1999. The stereoselective metabolism of fluoxetine in poor and extensive metabolizers of sparteine. Pharmacogenetics 9:55–60.

Goldney RD, Phillips PJ, Fisher LJ, Wilson DH. 2004. Diabetes, depression, and quality of life: A population study. Diabetes Care 27:1066–1070.

Gram LF, Overo K, Kirk L. 1974. Influence of neuroleptics and benzodiazepines on metabolism of tricyclic antidepressants in man. American Journal of Psychiatry 131:863–866.

Guengerich FP. 1997. Role of cytochrome P450 enzymes in drug–drug interactions. Advance in Pharmacology 43:7–35.

Harten J. 1995. Overview of the pharmacokinetics of fluvoxamine. Clinical Pharmacokinetics 29:1–9.

Ito K, Ogihara K, Kanamitsu S, Itoh T. 2003. Prediction of the in vivo interaction between midazolam and macrolides based on in vitro studies using human liver microsomes. Drug Metabolism and Disposition 31:945–954.

Kanamitsu S, Ito K, Okuda H, Ogura K, Watabe T, Muro K, Sugiyama Y. 2000. Prediction of in vivo drug–drug interactions based on mechanism-based inhibition from in vitro data: Inhibition of 5-fluorouracil metabolism by (E)-5-(2-bromovinyl) uracil. Drug Metabolism and Disposition 28:467–474.

Kato K, Yasui N, Fukasawa T, Aoshima T, Suzuki A, Kanno M, Otani K. 2003. Effects of itraconazole on the plasma kinetics of quazepam and its two active metabolites after a single oral dose of the drug. Therapeutic Drug Monitoring 25:473–477.

Kaye CM, Haddock RE, Langley PF, Mellows G, Tasker TC, Zussman BD, Greb WH. 1989. A review of themetabolism and pharmacokinetics of paroxetine in man. Acta Psychiatrica Scandinavica Supplementum 350:60–75.

Kerr BM, Thummel KE, Wurden CJ, Klein SM, Kroetz DL, Gonzalez FJ, Levy RH. 1994. Human liver carbamazepine metabolism. Role of CYP3A4 and CYP2C8 in 10,11-epoxide formation. Biochemical Pharmacology 47:1969–1979.

Kobayashi K, Chiba K, Yagi T, Shimada N, Taniguchi T, Horie T, Tani M, Yamamoto T, Ishizaki T, Kuroiwa Y. 1997. Identification of cytochrome P450 isoforms involved in citalopram N-demethylation by human liver microsomes. Journal of Pharmacology and Experimental Therapeutics 280:927–233.

Kobayashi K, Ishizuka T, Shimada N, Yoshimura Y, Kamijima K, Chiba K. 1999. Sertraline N-demethylation is catalyzed by multiple isoforms of human cytochrome P-450 in vitro. Drug Metabolism and Disposition 27:763–766.

Kugaya A, Akechi T, Okuyama T, Nakano T, Mikami I, Okamura H, Uchitomi Y. 2000. Prevalence, predictive factors, and screening for psychologic distress in patients with newly diagnosed head and neck cancer. Cancer 88:2817–2823.

Kurtz DL, Bergstrom RF, Goldberg MJ, Cerimele BJ. 1997. The effect of sertraline on the pharmacokinetics of desipramine and imipramine. Clinical Pharmacology and Therapeutics 62:145–156.

Labbé L, Turgeon J. 1999. Clinical pharmacokinetics of mexiletine. Clinical Pharmacokinetics 37:361–384.

Lane RM. 1996. Pharmacokinetic drug interaction potential of selective serotonin reuptake inhibitors. International Clinical Psychopharmacology 11:31–61.

Levine B, Jenkins AJ, Smialek JE. 1994. Distribution of sertraline in postmortem cases. Journal of Analytical Toxicology 18:272–274.

Lin JH, Lu AY. 1998. Inhibition and induction of cytochrome P450 and the clinical implications. Clinical Pharmacokinetics 35:361–390.

Margolis JM, O'Donnell JP, Mankowski DC, Ekins S, Obach RS. 2000. (R)-, (S)-, and racemic fluoxetine N-demethylation by human cytochrome P450 enzymes. Drug Metabolism and Disposition 28:1187–1191.

Mayhew BS, Jones DR, Hall SD. 2000. An in vitro model for predicting in vivo inhibition of cytochrome P450 3A4 by metabolic intermediate complex formation. Drug Metabolism and Disposition 28:1031–1037.

Nakajima M, Kobayashi K, Shimada N, Tokudome S, Yamamoto T, Kuroiwa Y. 1998. Involvement of CYP1A2 in mexiletine metabolism. British Journal of Clinical Pharmacology 46:55–62.

Nakajima M, Suzuki M, Yamaji R, Takashina H, Shimada N, Yamazaki H, Yokoi T. 1999. Isoform selective inhibition and inactivation of human cytochrome P450s by methylenedioxyphenyl compounds. Xenobiotica 29:1191–1202.

Nyberg G, Axelsson R, Martensson E. 1978. Binding of thioridazine and thioridazine metabolites to serum proteins in psychiatric patients. European Journal of Clinical Pharmacology 14:341–350.

Okamura H, Watanabe T, Narabayashi M, Katsumata N, Ando M, Adachi I, Akechi T, Uchitomi Y. 2000. Psychological distress following first recurrence of disease in patients with breast cancer: Prevalence and risk factors. Breast Cancer Research and Treatment 61:131–137.

Ortiz de Montellano PR, Correia MA. 1995. Inhibition of cytochrome P450 enzymes. In: PR Ortiz de Montellano, editor. Cytochrome P450 structure, mechanism and biochemistry. New York: Plenum. pp 305–366.

Otani M, Fukuda T, Naohara M, Maune H, Senda C, Yamamoto I, Azuma J. 2003. Impact of CYP2D6*10 on mexiletine pharmacokinetics in healthy adult volunteers. European Journal of Clinical Pharmacology 59:395–399.

Paczkowski D, Sadowski Z, Filipek M, Kolinski P. 1990. Pharmacokinetics of mexiletine and its metabolites, hydroxymethylmexiletine and p-hydroxymexiletine, after single oral administration in healthy subjects. Polish Journal of Pharmacology and Pharmacy 42:365–375.

Pan LP, Wijnant P, Vriendt C, Rosseel MT, Belpaire FM. 1997. Characterization of the cytochrome P450 isoenzymes involved in the in vitro N-dealkylation of haloperidol. British Journal of Clinical Pharmacology 44:557–564.

Preskorn SH. 1998. Debate resolved: There are differential effects of serotonin selective reuptake inhibitors on cytochrome P450 enzymes. Journal of Psychopharmacology 12:S89–97.

Ring BJ, Catlow J, Lindsay TJ, Gillespie T, Roskos LK, Cerimele BJ, Swanson SP, Hamman MA, Wrighton SA. 1996. Identification of the human cytochromes P450 responsible for the in vitro formation of the major oxidative metabolites of the antipsychotic agent olanzapine. Journal of Pharmacology and Experimental Therapeutics 276:658–666.

Sallee FR, Pollock BG. 1990. Clinical pharmacokinetics of imipramine and desipramine. Clinical Pharmacokinetics 18:346–364.

Segel IH, editor. 1993. Rapid equilibrium partial and mixed type inhibition. In: Enzyme kinetics. New York: Wiley-Interscience. pp 161–226.

Silverman RB, editor. 1988. Mechanism-based enzyme inactivation. In: Chemistry and enzymology. Vol. 1. Boca Raton, FL: CRC Press. pp 3–30.

Skjelbo E, Brosen K. 1992. Inhibitors of imipramine metabolism by human liver microsomes. British Journal of Clinical Pharmacology 34:256–261.

Uchitomi Y, Mikami I, Nagai K, Nishiwaki, Y, Akechi T, Okamura H. 2003. Depression and psychological distress in patients during the year after curative resection of non-small-cell lung cancer. Journal of Clinical Oncology 21:69–77.

Vanderheeren FA, Muusze RG. 1977. Plasma levels and half lives of thioridazine and some of its metabolites I. High doses in young acute schizophrenics. European Journal of Clinical Pharmacology 11:135–140.

Vermeulen T. 1998. Distribution of paroxetine in three postmortem cases. Journal of Analytical Toxicology 22:541–544.

Von Moltke LL, Greenblatt DJ, Court MH, Duan SX, Harmatz JS, Shader RI. 1995. Inhibition of alprazolam and desipramine hydroxylation in vitro by paroxetine and fluvoxamine: Comparison with other selective serotonin reuptake inhibitor antidepressants. Journal of Clinical Psychopharmacology 15:125–131.

TOXICOLOGICAL SCIENCES 87(1), 296–305 (2005)
doi:10.1093/toxsci/kfi235
Advance Access publication June 23, 2005

Relationship between Hepatic Gene Expression Profiles and Hepatotoxicity in Five Typical Hepatotoxicant-Administered Rats

Keiichi Minami,* Toshiro Saito,† Masatoshi Narahara,† Hiroyuki Tomita,† Hirokazu Kato,† Hisashi Sugiyama,† Miki Katoh,* Miki Nakajima,* and Tsuyoshi Yokoi*,[1]

*Drug Metabolism and Toxicology, Division of Pharmaceutical Sciences, Kanazawa University, Kanazawa, Japan, and †Life science group, Hitachi Ltd., Saitama, Japan

Received May 27, 2005; accepted June 2, 2005

In the field of gene expression analysis, DNA microarray technology has a major impact on many different areas including toxicogenomics, such as in predicting the adverse effects of new drug candidates and improving the process of risk assessment and safety evaluation. In this study, we investigated whether there is relationship between the hepatotoxic phenotypes and gene expression profiles of hepatotoxic chemicals measured by DNA microarray analyses. Sprague-Dawley rats (6 weeks old) were administered five hepatotoxicants: acetaminophen (APAP), bromobenzene, carbon tetrachloride, dimethylnitrosamine, and thioacetamide. Serum biochemical markers for liver toxicity were measured to estimate the maximal toxic time of each chemical. Hepatic mRNA was isolated, and the gene expression profiles were analyzed by DNA microarray containing 1,097 drug response genes, such as cytochrome P450s, other phase I and phase II enzymes, nuclear receptors, signal transducers, and transporters. All the chemicals tested generated specific gene expression patterns. APAP was sorted to a different cluster from the other four chemicals. From the gene expression profiles and maximal toxic time estimated by serum biochemical markers, we identified 10 up-regulated genes and 10 down-regulated genes as potential markers of hepatotoxicity. By Quality-Threshold (QT) clustering analysis, we identified major up- and down-regulated expression patterns in each group. Interestingly, the average gene expression patterns from the QT clustering were correlated with the mean value profiles from the biochemical markers. Furthermore, this correlation was observed at any extent of hepatotoxicity. In this study, we identified 17 potential toxicity markers, and those expression profiles could estimate the maximal toxic time independently of the hepatotoxicity levels. This expression profile analysis could be one of the useful tools for evaluating a potential hepatotoxicant in the drug development process.

Key Words: gene expression profiles; hepatotoxicity; DNA microarray.

The aim of toxicological studies is to detect adverse effects of a chemical on an organism based on observed toxicity markers (i.e., serum biochemical markers and chemical-specific gene expression) or phenotypic outcomes. In the past several years, novel systems, especially microarray technology, have been developed, allowing the simultaneous measurement of gene expression at the RNA level. Microarray technology can be used to elucidate the mechanisms of chemical-induced toxicity and have the possibility of being used as a tool for predicting the adverse effects of new drug candidates and improving the process of risk assessment and safety evaluation.

The liver is one of the first organs to be exposed to peroral-administered chemicals via the portal vein. Chemical concentrations in the liver are often much higher than the peak plasma concentration. The liver is also the major site for xenobiotic metabolism, and various chemicals can lead to the formation of active metabolites with toxic effects. The high concentration exposure and metabolic activity make the liver one of the primary targets for various types of chemical-induced toxicity.

The five typical hepatotoxicants chosen in this study were acetaminophen (APAP, *p*-acetamidophenol), bromobenzene (BB), carbon tetrachloride (CT), dimethylnitrosamine (DMN), and thioacetamide (TA). APAP is known as a mild analgesic drug, but it is a potent hepatotoxicant at high doses and in persons with enhanced susceptibility. APAP is largely (apparently more than 80%) converted to conjugates of glucuronate and sulfate. A minor amount, less than 5%, is metabolized to an active metabolite, mainly *N*-acetyl-*p*-benzoquinone imine (NAPQI) by cytochrome P450 (CYP) 2E1, which binds promptly to glutathione (GSH). Other metabolites (5 to 15%) appear to have no toxicity (Zimmerman, 1999). When an active metabolite exceeds the GSH content, excess metabolite binds to tissue molecules and manifests toxicity such as necrosis. BB, a traditional hepatotoxicant, is subjected to cytochrome P450-mediated epoxidation, and a major metabolite is 3,4-epoxide. Detoxication of the active metabolite is by GSH conjugation. At high BB doses, due to the conjugation to the epoxides, liver GSH shortage and secondary reactions such as lipid peroxidation, intracellular calcium alteration, and mitochondrial dysfunction

[1] To whom correspondence should be addressed at Drug Metabolism and Toxicology, Division of Pharmaceutical Sciences, Kanazawa University, Kakuma-machi, Kanazawa 920-1192, Japan. Fax: +81-76-234-4407. E-mail: tyokoi@kenroku.kanazawa-u.ac.jp.

© The Author 2005. Published by Oxford University Press on behalf of the Society of Toxicology. All rights reserved.
For Permissions, please email: journals.permissions@oupjournals.org

finally lead to cell death (Heijne *et al.*, 2003, Zimmerman, 1999). CT is a potent hepatotoxicant, and a single dose leads promptly to severe necrosis and steatosis. CT liver necrosis is caused by trichloromethyl free radicals from a CYP2E1-mediated pathway. The covalent binding of trichloromethyl to cell protein is considered the initial step of sequential events leading to membrane lipid peroxidation and, finally, to cell necrosis (Jeong, 1999; Zimmerman, 1999). DMN is the most potent toxicant of all dialkylnitrosamines and leads to hemorrhagic necrosis and steatosis. The DMN toxicity process is as follows: first, demethylation of CYP2E1 to monomethylnitrosamine; second, spontaneous change of diasomethane; finally, methylation of cell components (Zimmerman, 1999). Thioacetamide (TA) is a potent hepatotoxicant that requires metabolic activation by mixed-function oxidases. Generally, CYP2B, CYP2E1, and FMOs metabolize TA to its toxic metabolites (Hunter *et al.*, 1977; Wang *et al.*, 2000), and these intermediate metabolites might bind to cellular proteins by the formation of acetylimidolysine derivatives (Dyroff and Neal, 1981). TA is apparently converted to thioacetamide-*S*-oxide and is presumably converted to an active toxic metabolite that binds covalently to tissue molecules, provoking necrosis (Zimmerman, 1999).

The aims of this study were to find available toxicity marker genes, to investigate the correlation between biochemical markers and gene expression profiles, and to create a new evaluation method using DNA microarray. In this study, we attempted to apply our microarray of drug-response gene expressions for the evaluation of chemical-induced hepatotoxicity in rats.

MATERIALS AND METHODS

Animals and chemicals. Male Sprague-Dawley rats (5-week old, 130–150 g) were obtained from SLC Japan (Hamamatsu, Japan). Animals were housed in a controlled environment (temperature 25 ± 1°C, humidity 50 ± 10%, and 12-h light/12-h dark cycle) in the institutional animal facility with access to food and water *ad libitum*. Animals were acclimatized for a week before use in experiments. Animal maintenance and treatment were conducted in accordance with the National Institutes of Health Guide for Animal Welfare of Japan, as approved by Institutional Animal Care and Use Committee of Kanazawa University, Japan. APAP, BB, CT, DMN, and TA were obtained Wako Pure Chemical Industries (Osaka, Japan). ISOGEN, RNA extraction reagent was from Nippon Gene (Tokyo, Japan). *N*-hydroxysuccinimide (NHS)-ester Cy3 or Cy5 was from GE Healthcare Amersham Biosciences (Buckinghamshire, UK). ReverTra Ace (Moloney Murine Leukemia Virus Reverse Transcriptase RnaseH Minus) was from Toyobo (Tokyo, Japan). Random hexamer and SYBR® Premix Ex Taq™ (Perfect Real Time) were from Takara (Osaka, Japan). All primers were commercially synthesized at Hokkaido System Sciences (Sapporo, Japan). Other chemicals were of the highest grade commercially available.

Administration of chemicals and assessment of liver injury. Eighty-eight rats were assigned to 22 groups (four rats/group). The dosing solutions were prepared as follows with each vehicle. APAP: 500 mg/kg in corn oil; BB: 2.5 mmol/kg in corn oil; CT: 1 ml/kg in corn oil; DMN: 20 mg/kg in saline; TA: 400 mg/kg in saline; control: vehicle for saline or corn oil group. The chemicals were intraperitoneally injected in a single bolus at a volume of 2 ml/kg. At the indicated time (6, 12, 24, 48 h after administration), the rats were sacrificed, and the liver and serum samples were collected. Four typical biochemical markers for hepatotoxicity (aspartate aminotransferase, AST; alanine aminotransferase, ALT; lactate dehydrogenase, LDH; alkaline phosphatase, ALP) were measured by SRL, Inc. (Tokyo, Japan).

RNA isolation. Total hepatic RNA was isolated using ISOGEN. Approximately 100 mg of whole liver were lysed with 1.0 ml of the lysis solution. Chloroform (200 µl) was added and vortexed vigorously for 15 s. The mixture was centrifuged at 15,000 × *g* for 15 min at 4°C. The aqueous phase was transferred carefully to a new tube, and the RNA was precipitated with 0.5 ml of isopropyl alcohol for 10 min at room temperature. The mixture was centrifuged at 15,000 × *g* for 10 min. After washing with 75% ethanol, the pellet was dissolved in diethylpyrocarbonate-treated water. Equal amounts of total mRNA from each hepatotoxicant-administered sample were pooled and used for the microarray analysis and real-time reverse transcriptase (RT)-PCR.

In vitro amplification and DNA microarray. cDNA targets were prepared from pooled total RNA by *in vitro* transcription reaction as described previously (Luo *et al.*, 1999). Amplified RNA (6 µg) was reverse transcribed by random hexamer and aminoallyl-dUTP. The synthesized cDNA was labeled with NHS-ester Cy3 or Cy5 (Hughes *et al.*, 2001). The labeled cDNA was applied to the cDNA microarray (Rat Drug Response Chip containing 1,097 genes, Hitachi, Tokyo, Japan). In order to confirm the microarray data in the APAP group, a Rat cDNA Microarray kit G4105A containing 14,815 genes (Agilent Technologies, Palo Alto, CA) was used. Hybridization was performed at 62°C for 14 h. After washing, the microarray was scanned on a ScanArray 5000 (Packard BioChip Technologies, Billerica, MA), and the image was analyzed using QuantArray software (Packard BioChip Technologies). The signal intensity of each spot was calibrated by subtraction of the intensity of the control.

Real-time RT-PCR. Rat Cathepsin L (CtsL), Diazepam binding inhibitor (Dbi), Heme oxygenase 1 (Hmox1), Sulfotransferase 1a2 (Sult1a2), T-cell death associated gene (Tdag), and GAPDH were quantified by real-time RT-PCR. Primer sequences using in this study were as follows: CtsL, 5′-TCT ACT ATG AAC CCA ACT G-3′ and 5′-GAT TCA AGT ACC ATG GTC T-3′; Dbi, 5′-CCA ACT GAT GAA GAG ATG CTG T-3′ and 5′-CCC TAA CAT ATC AGA GCC ATG T-3′; Hmox1, 5′-ATA GAG CGA AAC AAG CAG A-3′ and 5′-TAG AGC TGT TTG AAC TTG G-3′; Sult1a2, 5′-TCA TTG AGT GGA CTT TGC CTT-3′ and 5′-CAC TTT TCC AGC TTT GAA CTG-3′; Tdag, 5′-CCA AGC AGG TAC AAC ATC AG-3′ and 5′-TTC TGC CTC GTA GAC TTG AC-3′. For RT process, total RNA (4 µg) and 150 ng random hexamer were mixed and incubated at 70°C for 10 min. RNA solution was added to a reaction mixture containing 100 units of ReverTra Ace, reaction buffer, and 0.5 mM dNTPs in a final volume of 40 µl. The reaction mixture was incubated at 30°C for 10 min, 42°C for 1 h, and heated at 98°C for 10 min to inactivate the enzyme. Real-time PCR was performed using the Smart Cycler® (Cepheid, Sunnyvale, CA) with Smart Cycler® software (Ver. 1.2b). PCR mixture contained 1 µl of template cDNA, SYBR® Premix Ex Taq™ solution and 10 pmol of sense and antisense primers. The PCR condition for GAPDH and Sult1a2 was as follows: after an initial denaturation at 95°C for 30 s, the amplification was performed by denaturation at 94°C for 4 s, annealing and extension at 64°C for 20 s for 45 cycles. The PCR condition for other genes was as follows: after an initial denaturation at 95°C for 20 s, the amplification was performed by denaturation at 95°C for 5 s, annealing at 55°C for 10 s, and extension at 72°C for 15 s for 45 cycles. Amplified products were monitored directly by measuring the increase of the dye intensity of the SYBR Green I (Molecular Probes, Eugene, OR) that binds to double-strand DNA amplified by PCR.

Data management. Fold-change determination, experiment normalization, and clustering analysis were performed with GeneSpring software (Agilent Technologies). Gene expression values for each chip were normalized to the intensity-dependent (LOWESS) normalization built in GeneSpring. In the Quality-Threshold (QT) clustering analyses, a standard correlation method was used in this study. Fold-change filters included the requirement that the

TABLE 1
Changes of Biochemical Markers in Five Chemical-Administered Rats

Chemical	Time(h)	AST (IU/l)	ALT (IU/l)	LDH (IU/l)	ALP (IU/l)
Control (corn oil)	48	152 ± 7	60 ± 3	2647 ± 248	1711 ± 128
Control (saline)	48	177 ± 22	55 ± 9	3528 ± 566	1499 ± 49
Acetaminophen (APAP)	6	239 ± 18[a]	72 ± 8	3590 ± 265	1184 ± 85[a]
	12	294 ± 66[a]	78 ± 13	4001 ± 480	1222 ± 53[a]
	24	187 ± 28	56 ± 7	4240 ± 1130	1478 ± 176
	48	248 ± 68	81 ± 17	3949 ± 684	1283 ± 123
Bromobenzene (BB)	6	177 ± 14	49 ± 5[a]	4088 ± 708	1625 ± 7
	12	178 ± 14	41 ± 1[b]	3891 ± 476	1239 ± 51[a]
	24	476 ± 88[a]	120 ± 23[a]	5785 ± 248[b]	1876 ± 181
	48	618 ± 206	259 ± 76[a]	4068 ± 1023	1403 ± 163
Carbon tetrachloride (CT)	6	1196 ± 155[b]	411 ± 75[b]	6284 ± 962[a]	1638 ± 207
	12	782 ± 317	303 ± 147	4079 ± 399	1123 ± 46[a]
	24	595 ± 163[a]	248 ± 94	3533 ± 579	1154 ± 112[a]
	48	2059 ± 651[a]	706 ± 156[b]	3120 ± 487	1328 ± 170
Dimethylnitrosamine (DMN)	6	217 ± 26	60 ± 8	2933 ± 558	1516 ± 144
	12	266 ± 70	84 ± 24	2278 ± 303	1486 ± 314
	24	186 ± 15	88 ± 5[a]	1038 ± 153[b]	1848 ± 187
	48	426 ± 28[b]	192 ± 24[b]	846 ± 21[b]	1182 ± 100
Thioacetamide (TA)	6	198 ± 8	52 ± 2	3586 ± 429	1344 ± 149
	12	287 ± 18[b]	75 ± 4	3180 ± 239	1817 ± 53[b]
	24	8312 ± 1735[b]	1749 ± 371[b]	53083 ± 9662[b]	1682 ± 89
	48	1933 ± 405[b]	487 ± 91[a]	3976 ± 219	2174 ± 342

Note. Data are expressed as mean ± SE ($n = 4$).
[a]Significantly different from control group ($p < 0.05$).
[b]Significantly different from control group ($p < 0.01$).

genes be present in at least 200% of the administered samples for up-regulated genes, and 50% of controls for down-regulated genes.

Statistics. The *t*-test was used to detect significant differences between the means of two groups relative to the observed variance within groups.

RESULTS

Assessment of Liver Toxicity

The serum biochemical markers in the five chemical-administered groups were measured at 6, 12, 24, and 48 h after administration (Table 1). The AST activities of the APAP-, BB-, CT-, DMN-, and TA-administered groups were significantly high at 12, 24, 6, 48, and 24 h after administration, respectively. The changes of the ALT activities showed almost the same pattern as the AST activities in all groups. The LDH activity increased significantly in the BB-, CT-, and TA-administered groups at 24, 6, and 24 h, respectively. In the DMN-administered group, the LDH activity significantly decreased at 24 and 48 h in a time-dependent manner. In the APAP-administered group, no significant change was observed. The ALP activity decreased significantly in the APAP-, BB-, and CT-administered groups at 6 and 12, 12, and 12 and 24 h, respectively. In the TA-administered group, the ALP activity significantly increased at 12 h. In the DMN-administered group, no significant change of the ALP activity was observed. Taking these results into consideration, the maximal toxic times of APAP, BB, CT, DMN, and TA were estimated as 12, 24, 6, 48, and 24 h, respectively.

Genes Significantly Changed by at Least Four Chemicals at the Toxic Time Points

Analysis of the gene expression profile showed that 52 (25 up-regulated and 27 down-regulated) of 1,097 genes were changed above 2-fold by at least four chemicals at the maximal toxic times described above (Table 2). Eleven genes were changed above 2-fold in all the chemical administered groups (3 up-regulated and 8 down-regulated, Table 2), and 40 genes in four of the five chemical administered groups (21 up-regulated and 19 down-regulated, Table 2).

The genes in Table 2 are presented by two-way hierarchical clustering (Fig. 1). In the up-regulated genes at the maximal toxic times (Fig. 1A), CT-, TA-, and BB-administered groups were sorted in a similar cluster. However, all APAP-administered groups were sorted in a different cluster from other groups. The DMN-administered groups from 12 to 48 h were sorted in a similar cluster. Among the down-regulated genes at the maximal toxic times (Fig. 1B), those of the CT- and TA-administered groups, BB- and DMN-administered groups, and APAP-administered groups were sorted in a similar cluster,